Control of relative radiation pressure in optical traps: Application to phagocytic membrane binding studies

Holger Kress,* Ernst H. K. Stelzer, Gareth Griffiths, and Alexander Rohrbach†
European Molecular Biology Laboratory (EMBL), Meyerhofstrasse 1, D-69117 Heidelberg, Germany
(Received 14 February 2005; published 29 June 2005)

We show how to control the relative radiation pressure and thereby the stable trap position of an optically trapped bead by variation of the mean incident axial photon momentum. The thermal position fluctuations of a trapped bead are recorded by a three-dimensional back-focal-plane interferometry. The interferometric detection signals are in agreement with predictions based on an extended Mie theory. Depending on the application, the unique and linear range of such a detection system can be optimized by controlling the trap position of the bead. We use this method to investigate in three dimensions the binding of beads to membranes of living cells during phagocytosis. We found that independent of the bead coating (IgG, complement, LPS, avidin) the most frequent initial mechanical response of the cell was a downward pulling of the bead into the cell. The time delay between binding and response was on average 2 s.

DOI: 10.1103/PhysRevE.71.061927 PACS number(s): 87.80.Cc, 87.16.Dg, 42.79.Pw, 87.64.Cc

I. INTRODUCTION

Single-beam optical traps [1] have been widely used to trap and manipulate microscopic particles for many years [2,3]. Three-dimensional (3D) position detection systems enable the tracking of a trapped particle with nanometer precision at sampling rates of up to 1 MHz [4–7], enabling force measurements on the piconewton range in 3D. In the photonic force microscope (PFM) [6–8] a trapped particle acts as a probe which, driven by extended Brownian motion, scans its local environment. The thermal fluctuations of the particle are determined by its environment and are altered when external forces act on the fluctuating probe. The PFM is therefore a tool for measuring weak interactions between the trapped probe and its environment by recording the probe's 3D position fluctuations. The instrument is used to investigate diffusion in cell membranes [9], to image 3D cavity structures [10], and to study the mechanical properties of single molecules [11,12], as well as surface forces, molecular binding forces, and small variations in local diffusion and viscosity. Optical tweezers in combination with an interferometric quadrant photodiode (QPD) detection system were used to track the motion of single-molecular motors [13] and to investigate diffusion within living cells by microrheology [14].

If an optically trapped fluctuating bead is used as a local probe to image 3D interaction potentials, it is usually displaced from the trap center during the measurement. If the binding of a bead to a cell membrane is studied (Fig. 1), the bead is displaced from the trap center on the one hand due to the binding process itself. On the other hand, it is additionally displaced if the membrane moves the bound bead. However, the interferometric 3D position detection with the PFM is only unique and linear in limited regions around the trap center [15–17]. The unique detection region is the region where the position signals can be inverted in order to provide the unambiguous 3D bead position. In order to know whether the measured QPD signals reproduce the bead movement, it is important to know the exact size of the unique and linear region in three dimensions. A complementary approach to the static trap that is described here is the introduction of a force clamp feedback control system [3,18,19]. There, the time-averaged displacement of the bead is compensated by a deflection of either the optical trap or the sample stage. However, a trap displacement such as by scanning mirrors is only possible in the lateral, but not in the axial direction. In addition, repeated stepwise repositioning of the trap or the sample causes an energetic disturbance of the system, which makes equilibrium measurements less reliable.

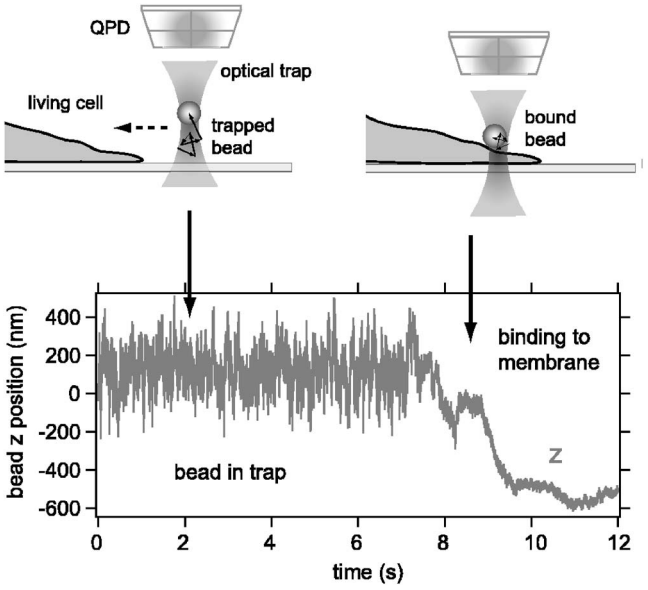

FIG. 1. Principle of the binding experiments. An optically trapped bead is moved to touch the plasma membrane of a living cell. The bead's thermal position fluctuations during the binding event are recorded in 3D by a quadrant photodiode (QPD).

*Electronic address: kress@embl.de
†Electronic address: rohrbach@embl.de

In the recent past, the influence of the QPD *detection optics* has been investigated theoretically [15,16] and experimentally [20] in order to improve 3D particle tracking. In this article we show how the 3D position detection system can be tuned to the particular experimental situation by regulating the *optical interaction* between the laser beam and the trapped bead. We show how to control the relative radiation pressure and thereby the stable trap position of the bead by variation of the mean incident axial photon momentum. This variation is equivalent to a change of the mean axial wavelength of the laser in the focal region. This change can be described by a change of the Gouy-Phase shift [21,22], which alters the interference pattern on the QPD and thereby the position detection signals. By changing the axial trap position of the bead, the detector signals can be optimized for the specific application.

We used the improved 3D position tracking capability of the PFM to investigate the dynamics of bead binding to a cell membrane (Fig. 1). In particular, we studied the initial binding of a bead to the membrane preceding its uptake into a macrophage by phagocytosis.

Phagocytosis is a central cellular mechanism in the innate mammalian immune system. Although many cell types can undergo this process under some conditions, it is a major function of the three so-called "professional" phagocytes: macrophages, neutrophils, and dendritic cells [23]. When an invading pathogen, such as a bacterium, binds to the membrane of a macrophage, ligands on the particle interact with cell surface receptors to initiate a complex process in which the plasma membrane wraps around the invader [24]. The bacterium is then internalized into a membrane-enclosed compartment, the phagosome where the pathogen can be degraded [24]. Besides bacteria, macrophages also take up senescent cells or latex beads, which have been shown in many studies [25] to be excellent models for some bacterial infections.

In the recent past, Caspi *et al.* [26,27] investigated by video microscopy the intracellular retrograde transport of engulfed beads after placing them on top of the membrane by means of optical tweezers. Choquet *et al.* [28] and Takahashi *et al.* [29] studied the extracellular movement of beads attached to the cell membrane by optical tweezers. In all these cases, the bead movement was tracked laterally in two dimensions. However, no study was made on the 3D dynamics of the Brownian-motion-driven binding and the initial mechanical response of the membrane. We investigate these processes using the fast (kHz–MHz) and precise (nm) 3D tracking system of the PFM.

This paper is organized as follows: In Sec. II we describe how to determine the linear and the unique range of the QPD detection system. The experimental interferometric detector signals are compared to theoretical predictions [15,16]. Section III presents a method to control the relative radiation pressure exerted on a trapped bead and thereby its trapping position. We show that the trapping position is related to the extent of the unique detector range. Thus, by controlling the relative radiation pressure, it is possible to control the unique detector range. Finally Sec. IV shows the application of photonic force microscopy to study the dynamics of beads binding to the membrane of macrophage cells. We investigate the dynamics of the binding process, the initial mechanical response of the membrane upon binding, and the time delay between binding and membrane response.

II. INTERFEROMETRIC POSITION DETECTION

A. Position detection signals

A bead that is trapped by a focused laser beam scatters a fraction of the incident light. The scattering spectrum depends on the bead position $\mathbf{b}=(b_x,b_y,b_z)$ relative to the geometric focus. The scattered light interferes with the unscattered light and is imaged by a detection lens onto a QPD, which is placed in the back-focal plane (BFP) of the lens [7]. Linear combinations of the four QPD signals yield two lateral position signals $S_x(\mathbf{b})$ and $S_y(\mathbf{b})$ and an axial position signal $S_z(\mathbf{b})$. In the case of a trapped spherical bead, these signals are linear with the displacement of the bead within a restricted region [15–17,20]. In the case of elongated objects, these signals also depend on the object's orientational fluctuation [30].

The first step in order to determine the unique and linear range of the detection signal is to scan a bead through the focus. This can be done by fixing a bead to the coverslip and moving the piezostage with the coverslip through the focal region of the trapping beam. In order to enable binding between the bead and coverslip, the immersion medium has to contain a sufficiently high ion concentration to shield the electrostatic repulsion. We used a $10\times$ PBS solution (phosphate buffer saline, ion concentration 1.5 M) for that purpose.

We checked the influence of the coverslip on the detection signals by comparing the signals of a bead fixed on a coverslip to the signals of a bead that was immobilized in a 0.5% agarose gel. At that concentration, the agarose gel changes the refractive index of pure water or PBS only marginally. There was no significant difference between the detector signals obtained from a bead attached to a coverslip and a bead immobilized in agarose.

The trapping laser had a wavelength of $\lambda_0=1064$ nm in air, the water immersion trapping lens a numerical aperture $\mathrm{NA}_{trap}=1.2$ in water. The immersion medium was either PBS or nutrition medium for the experiments without and with living cells, respectively. Polystyrene (latex) beads with a diameter of 1.03 μm and a refractive index of $n=1.57$ were used. The trapping lens was overilluminated with a Gaussian beam with a beam waist radius twice that of the entrance pupil of the trapping lens. The numerical aperture of the detection lens was adjusted to $\mathrm{NA}_{det}=0.47$ [7].

We measured the detector response for 2D scanning (xz plane) and one-dimensional scanning (z direction). Figure 2 shows the 2D position signals of a bead as it is scanned in the xz plane through the focus. Displayed are the x and z signals of the QPD as a function of the bead's x and z position.

The measured detector response was compared to theoretical predictions based on extended Mie calculations [15,16]. The z signal S_{az} as a function of the bead position $\mathbf{b}$ is

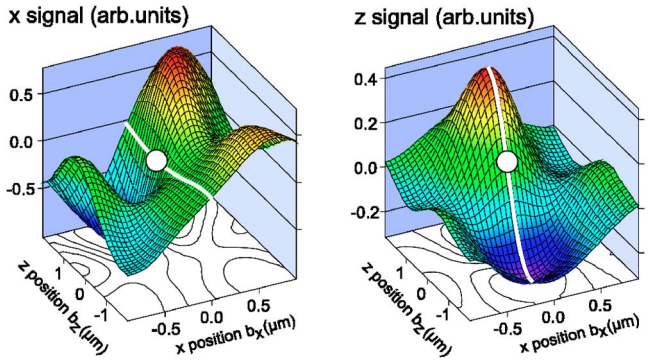

FIG. 2. (Color online) Experimental two-dimensional QPD position signals. A bead fixed to a coverslip is scanned through the focal region in the xz plane. The left and right plots show the x and z signals, respectively. The b_z position offset is chosen arbitrarily.

$$S_{az}(\mathbf{b}) = a\epsilon_0 c \int\int_{k_\perp < k_0 \mathrm{NA}_{det}} |\tilde{E}_i(k_x,k_y)\Theta(k_0 \mathrm{NA}_{trap} - k_\perp) + \tilde{E}_s(k_x,k_y,\mathbf{b})|^2 dk_x dk_y, \quad (1)$$

where $\tilde{E}_i$ and $\tilde{E}_s$ are the angular spectra (2D Fourier transforms) of the incident electric field and the field that is scattered by the bead, respectively. k_x and k_y are the x and y components and $k_\perp = (k_x^2 + k_y^2)^{1/2}$ the lateral component of the wave vector. The wavelength of the laser light λ_0 determines the wave number $k_0 = 2\pi/\lambda_0$. Θ is the Heaviside unit step function, which cuts off the field at the BFP or a conjugate plane of the trapping lens. The prefactors of the integral are the speed of light c, the dielectric constant ϵ_0, and an arbitrary factor a that accounts for the sensitivity of the QPD and the electronic amplification of the signal. The subscript a in the notation of the z signal S_{az} shall clarify that the signal is not normalized like in previous articles [15,16].

One of the parameters in Eq. (1) that can be controlled experimentally is NA_{trap}, which determines the Gouy phase shift and thereby the interference pattern on the QPD. We compared the theoretical predictions from Eq. (1) with the experimental data for various NA_{trap} values. Figure 3 shows the measured and theoretical z signal $S_{az}(b_z)$ of a bead scanned along the optical axis for $\mathrm{NA}_{trap}=1.2$ (top graph) and $\mathrm{NA}_{trap}=0.86$ (middle graph). The measured signals are amplified electronically with a factor we did not determine. Therefore, for the comparison between theory and experiment the factor a in Eq. (1) and an arbitrary offset added to the signal S_{az} were fitted.

One characteristic value of the detector signal is the distance d_{MM} between the minimum and maximum of S_{az}. This value, which is the size of the unique detector region in the z direction, increases with decreasing NA_{trap}. The bottom graph of Fig. 3 shows the measured and experimental values of d_{MM} as a function of NA_{trap}. In addition, the NA_{trap}-dependent axial extent

$$r_z = \frac{\lambda_0}{n(1-\cos\alpha)} \quad (2)$$

of the focal spot is plotted. Here, n is the refractive index of the immersion medium and α the opening angle of the trapping lens with $\mathrm{NA}_{trap} = n \sin\alpha$.

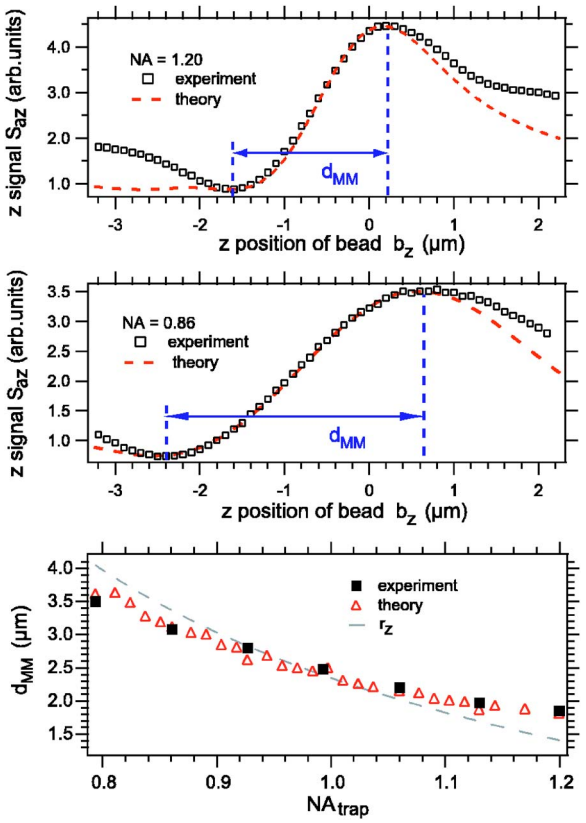

FIG. 3. (Color online) Comparison between experiment and theory for the axial position signal S_{az}. S_{az} is shown as a function of the bead's z b_z position for $\mathrm{NA}_{trap}=1.2$ (top graph) and $\mathrm{NA}_{trap}=0.86$ (middle graph). The bottom graph shows the distance d_{MM} from the minimum to the maximum of S_{az} as a function of NA_{trap}. The dashed line is the theoretical axial extent of the focal light distribution.

B. Trapping position and unique detector range

The white lines at $b_x=0$ μm in Fig. 2 (left and right) correspond to the optical axis, the z axis. The $b_z=0$ μm position is chosen arbitrarily since it is not known where the geometrical focus is located within the detector response. Using the method of local mean-square displacement (local MSD) [17] it is possible to check whether the detector signals are linear at least within the optical trapping volume. For a 1-μm latex sphere trapped using a $\mathrm{NA}_{trap}=1.2$ lens and a laser power of 2 mW in the focal plane, the widths of the approximately Gaussian-shaped trap volume are $\sigma_{xy} \approx 30$ nm and $\sigma_z \approx 70$ nm. By using local MSD, we found that the detector signals are linear within this region. Therefore, and due to the lateral symmetry of the focus, one can assume that the bead is trapped somewhere along the white line between the maximum and minimum of the z signal (Fig. 2, right). However, since the size of the linear detector region in all three dimensions depends strongly on the exact trapping position, it is necessary to identify this position.

The trapping position of a bead can be determined as described by Lang *et al.* [31]. As sketched in Fig. 4 (top graph, inset), a bead is tightly trapped a few micrometers above the coverslip. Then, the coverslip is moved upwards

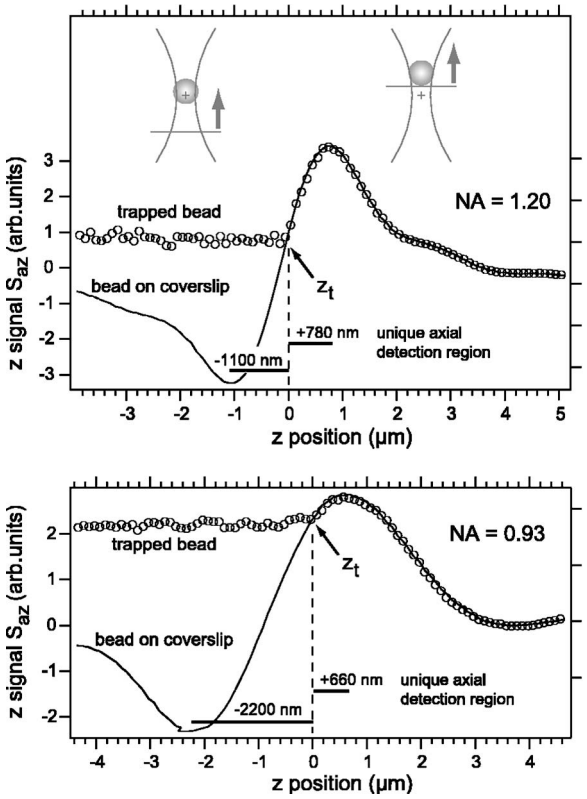

FIG. 4. Determination of the experimental trapping position z_t relative to the experimental detector response. A bead is trapped a few micrometers above the coverslip. The coverslip is moved upwards and pushes the bead that attaches to the coverslip in axial direction, while the detector signal S_{az} is recorded (open circles). The trapping position is determined by comparing these signals to those with a bead attached to the coverslip (solid line). The upper graph shows a measurement for a trapping $NA_{trap}=1.2$. The bottom graphs shows that z_t is shifted along the optical axis for a lower trapping $NA_{trap}=0.93$. The horizontal bars display the unique detection region in the $+z$ and $-z$ directions.

and pushes the bead that attaches to the coverslip in axial direction, while the detector signal S_{az} is recorded (Fig. 4, top graph, open circles). By comparing this signal with S_{az} of a bead fixed to the coverslip (Fig. 4, top graph, solid line), the trapping position z_t relative to the detector response can be identified. This position is marked by white circles in Fig. 2 (left and right graph). With known z_t, one can determine the unique and linear range of the detector along all three dimensions. The unique detection region in the direction i $(i=x,y,z)$ is the region between the minimum and maximum of the position signal S_{ai}. The linear range of the detector is of course smaller than the unique range. Figure 5 (top graph, solid line) shows the x signal S_{ax} as a function of the bead's x position b_x at $z=z_t$.

These measurements show that, starting from the trapping position z_t as reference point, the *unique* detector range for $NA_{trap}=1.2$ is ±310 nm along a lateral axis (Fig. 5, top graph), 780 nm in the positive z direction, and 1100 nm in the negative z direction (Fig. 4, top graph). The exact size of the *linear* range depends on the degree of deviation from linearity that is still accepted until the signal is considered to

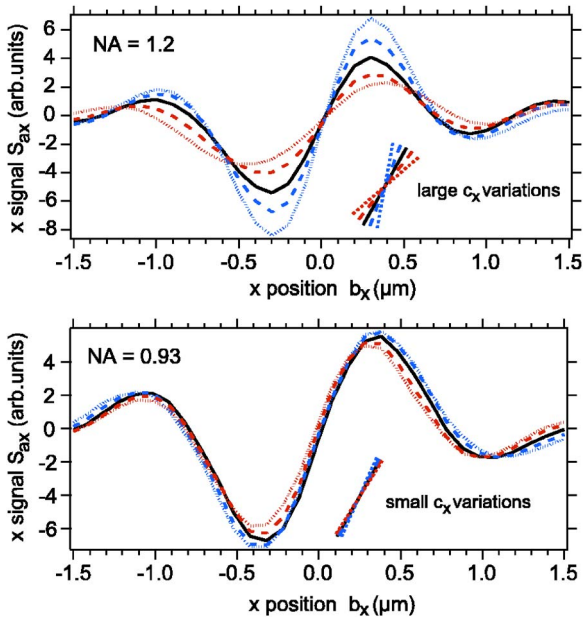

FIG. 5. (Color online) Change of the lateral signal sensitivity $c_x = dS_{ax}/db_x|_{\mathbf{b}=(0,0,b_z)}$ for different axial positions b_z. The top graph shows that for $NA_{trap}=1.2$, the lateral detector signal S_{ax} changes strongly if the bead is displaced from the trap center in axial direction (solid line, $b_z=z_t$; dashed lines, $b_z=z_t\pm200$ nm; dotted lines, $b_z=z_t\pm400$ nm; stronger signals for higher b_z values). For the lower $NA_{trap}=0.93$, the variations in c_x are significantly smaller (bottom graph).

be nonlinear. Due to this arbitrariness in the definition of linearity, we will in the following consider only the *unique* detector range, which is well defined.

C. Lateral signal sensitivity variations

In addition to the unique range, it is important to know whether the signal sensitivity dS_{ai}/db_i remains constant when the bead is moved away from the trap center. A very popular method for calibrating the position detection system is to calibrate the system while the bead is trapped in bulk solution by using the Langevin method [7,32]. As the trapped bead approaches an interaction partner its equilibrium position is changed in general. The easiest and most widely used approach is to assume that the QPD calibration factors $dS_{ai}/db_i|_{\mathbf{b}=(0,0,z_t)}$ determined at the trapping position $\mathbf{b}=(0,0,z_t)$ remain constant if the bead is moved away from the trap center [9–12]. Figure 5 (top) shows that the lateral x signal $S_{ax}(b_x)$ and thereby $c_x = dS_{ax}/db_x|_{\mathbf{b}=(0,0,b_z)}$ vary strongly (up to 60%) for various z displacements from the trap center ($b_z=z_t\pm200$ nm and ±400 nm). Once the variations in c_x (and also c_y, but for the sake of simplicity we consider in the following only the x direction) are known, one can correct the experimental data for this effect during the data analysis.

III. CONTROL OF RELATIVE RADIATION PRESSURE AND TRAPPING POSITION

A more elegant way to handle the problem of the variations in c_x would be to decrease these variations physically.

A closer evaluation of the detector response measurement in Fig. 2 (left graph) shows that the variations in c_x are rather strong at the trapping position (circle) but decrease further down the optical axis (at higher b_z values). Therefore, a way to get less variations in c_x is to shift the trapping position down the optical axis. Using the two-component approach, the total optical force $\mathbf{F}(\mathbf{b})$ acting on a small bead at the position $\mathbf{b}$ in an optical trap can be written as the sum of the gradient and the scattering force [33,34]

$$\mathbf{F}(\mathbf{b}) = \frac{1}{4V}\,\mathrm{Re}\int_V \underbrace{\alpha_0 \epsilon \nabla |\mathbf{E}_i(\mathbf{r})|^2}_{grad} + \underbrace{\alpha_0 \epsilon \nabla |\mathbf{E}_s(\mathbf{b},\mathbf{r})|^2 + \nabla [\mathbf{E}_i(\mathbf{r})\mathbf{E}_s^*(\mathbf{b},\mathbf{r}) + \mathbf{E}_s(\mathbf{b},\mathbf{r})\mathbf{E}_i^*(\mathbf{r})]}_{sca} d^3r. \tag{3}$$

with

$$\mathbf{E}_i(\mathbf{r}) = \frac{1}{(2\pi)^2}\int\int_{k_\perp < k_0 \mathrm{NA}_{trap}} \tilde{\mathbf{E}}_i(k_x,k_y)\exp[-i(xk_x + yk_y + z\sqrt{k_n^2 - k_\perp^2})]dk_x dk_y. \tag{4}$$

The first term corresponds the gradient force, which is proportional to the gradient of the focal intensity averaged over the particle volume and therefore directs towards the point of the highest focal intensity. The second term belongs to the scattering force, which in general pushes a particle along the optical axis. α_0 is the polarizability and V the volume of the particle; ϵ is the electric permittivity of the surrounding medium. The scattered field $\mathbf{E}_s(\mathbf{b},\mathbf{r})$ at point $\mathbf{r}=(x,y,z)$ depends also on the particle position $\mathbf{b}$. The incident electromagnetic field $\mathbf{E}_i(\mathbf{r})$ can be written as shown in Eq. (4) [33]. $\tilde{\mathbf{E}}_i(k_x,k_y)$ is, like in Eq. (1), the angular spectrum of the incident field at the BFP of the trapping lens. $k_n = k_0 n$ is the wave number in a medium with a refractive index n. In a stable trapping position of a particle, the gradient and scattering force cancel each other, resulting in a total optical force of zero. In general, a change of the relative radiation pressure (scattering force relative to gradient force) causes a shift of the force equilibrium position. A relative decrease of the gradient force or a relative increase of the forward pushing component of the scattering force moves the force equilibrium position along the optical axis in the direction of the beam propagation.

Such a shift of the trapping position down the optical axis in order to get lateral signals that hardly depend on b_z can be achieved by decreasing the angular spectrum of the electromagnetic field in the focal region. This change of the mean incident axial photon momentum is achieved by lowering NA_{trap}. Besides the shift of the trapping position, lowering NA_{trap} has an additional effect on decreasing the variations in c_x: a smaller NA_{trap} creates a more extended focal spot, yielding more extensive position signals.

Experimentally, NA_{trap} can be reduced by placing an aperture stop in a plane conjugate to the BFP of the trapping lens. Figure 4 shows that the trapping position is shifted if NA_{trap} is changed from 1.2 (top graph) to 0.93 (bottom graph). One the one hand, as expected, c_x was much more constant with respect to displacements in the z direction (Fig. 5, bottom) in the case of a $\mathrm{NA}_{trap}=0.93$. On the other hand, it can be seen in Fig. 4 that for the lower NA_{trap}, the trapping position is moved towards the maximum of S_{az}. The unique range of S_{az} in the positive z-direction is 660 nm and in the negative z direction 2200 nm. This means that the unique range in the $+z$ direction is decreased and in the $-z$ directions increased compared to $\mathrm{NA}_{trap}=1.20$. All these effects are also predicted by the extended Mie calculations described in [15,16].

We also measured the detection signals for an extremely small $\mathrm{NA}_{trap}=0.30$. We found that with such a small numerical aperture, optical trapping of 1-μm latex beads is no longer possible. However, for applications where the bead is restricted in motion by other forces, the fast and precise QPD tracking can still be used. The axial detector signal S_{az} was constant for an axial displacement of the bead and therefore not useful for position detection. But the lateral signal had a large unique range of ±900 nm and was constant over a very long axial range of about 5 μm.

The NA_{trap} dependence of the unique detector region and the c_x variations are summarized in Table I. It is shown that the c_x variations are small for low NA_{trap}. The unique detector region in the positive z direction is maximized with a large NA_{trap} whereas the unique detector region in the negative z direction is maximized with a small NA_{trap}. According to this table, the detection signals can be optimized depending on the specific application.

For the membrane binding experiments described in Sec. IV, a large unique detector region in all three dimensions and small c_x variations are required. As the optimal compromise for these requirements, $\mathrm{NA}_{trap}=1.06$ was chosen.

IV. APPLICATION TO PHAGOCYTIC MEMBRANE BINDING STUDIES

A. Phagocytosis

The phagocytic process can be divided into two major steps: first, the initial binding of the particle to the cell surface and formation of the phagosome and, second, the intracellular transport and maturation of the phagosome in the cell. Although the interferometric position detection system of the PFM can be used for intracellular tracking of beads or

TABLE I. The size of the unique detector region and the lateral signal sensitivity variations c_x depend on the trap position and therefore on NA_{trap}. Laterally, the extent of the unique detector region is symmetric in the $+x$ and $-x$ directions (Fig. 5). Axially, the unique region is larger along the $-z$ direction than along the $+z$ direction (Fig. 4).

	Unique detection region			
NA_{trap}	Lateral (nm)	Axial (nm)		c_x variations (%)[a]
1.2	±310	−1100	+780	16
1.13	±310	−1200	+760	10
1.06	±320	−1400	+770	8
0.99	±330	−1700	+750	6
0.93	±350	−2200	+660	2
0.86	±390	−2600	+470	1
0.74	±420	~−3500	~0	0
0.30	±900	0	0	0.01

[a]Variation of the lateral signal sensitivity $c_x = dS_{ax}/db_x|_{b=(0,0,b_z)}$ for an axial displacement of 100 nm from the trap position ($b_z = z_t \pm 100$ nm).

bacteria (see [35] for 2D tracking), we focus here on the initial phagocytic binding process.

The phagocytic response of the cell is triggered by ligands on the particle binding to and activating cell surface receptors. In order to ingest the particle, the membrane has to wrap around the particle. According to the current view, the morphology of the wrapping process depends on the cell membrane receptors involved in the binding process [36–38] (see sketch in Fig. 6). In our study we used four different types of ligands on beads: immunoglobulin G (IgG), complement, bacterial lipopolysaccharide (LPS), and avidin.

In case of IgG-coated particles binding to Fc receptors, probably the best characterized phagocytic system [39], membrane protrusions called pseudopods tightly adhere to the particle and engulf it by fusing at their tips. In contrast, particles binding to complement receptors have been described to sink into the main cell body with less pseudopod formation and a less tightly adherent membrane [36–38]. LPS is supposed to bind to CD14 receptors in conjunction with Toll-like receptors [23]. As there is no evidence that there is any biotin on the surface of macrophages, avidin can be considered a nonspecific protein that binds to unknown receptors.

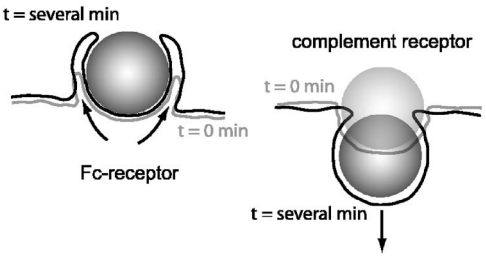

FIG. 6. Schematic of the current view of membrane morphology during Fc- and complement-receptor-mediated phagocytosis [36–38]. In the Fc-receptor case, growing pseudopods tightly adhere to the particle and engulf it by finally fusing at their tips. In the complement receptor case, the particle sinks into the cytoplasm.

So far, the morphological phagocytic membrane response was studied either by electron (see reviews [36,37]) or by fluorescence microscopy [41]. The latter study showed that the whole process of engulfment takes about 10 min. However, no investigation with a millisecond or microsecond sampling of the Brownian motion and a nanometer precision was made on the dynamics of the binding process and the following membrane response during the first few seconds after binding.

We applied the PFM to investigate the dynamics of membrane binding events during phagocytosis for different types of ligands on beads (IgG, complement, LPS, and avidin). With our study, we address the following questions: Over which time scale (milliseconds or seconds) does the binding to the membrane occur? What is the first mechanical response of the cell after the binding event? Does it depend on particle coating (IgG, complement, LPS, or avidin)? How long is the time delay between the binding and mechanical membrane response?

B. Materials and methods

We used 1.03-μm latex beads (Polysciences, Inc.), which have been shown in many studies [25] to be excellent models for some bacterial infections. The J774 [40] and RAW [41] mouse macrophages were obtained from ATCC and cultured as described. Cells were spread onto coverslips 1 day prior to the experiment. Three hours prior to the experiment, when the cells were about 30% confluent, the coverslips with 400 μl of medium were mounted into custom made aluminum coverslip holders and incubated in a wet chamber at 37 °C in a 5% CO_2 atmosphere. In the PFM, the cells were kept in a Hepes buffered medium at 37 °C by a custom-made heating system that minimizes thermal drifts of the piezostage.

The beads were added to the cells in a concentration that led to about 10–20 beads per cell. The beads were either coated with IgG (from murine serum, Sigma-Aldrich), complement (IgM from murine myeloma incubated with mouse serum [42], Sigma-Aldrich), bacterial LPS (from Klebsiella pneumoniae, Sigma-Aldrich), or avidin (Molecular Probes).

After addition of the beads, the cells were observed by DIC (differential interference contrast) video microscopy for about 15 min. After this time only those cells were chosen for the subsequent binding experiments that showed regular phagocytic behavior. A bead was optically trapped with $NA_{trap} = 1.06$ at a very low laser power of about 2 mW, resulting in optical force constants of $\kappa_{xy} \approx 6$ pN/μm in the lateral and $\kappa_z < 1$ pN/μm in the axial direction. The $NA_{trap} = 1.06$ was chosen for reasons discussed in Sec. III. The low laser power of 2 mW was used to minimize the possibility of radiation damage and to create a large trapping volume for extended Brownian motion prior to the binding.

The trapped bead was moved towards the membrane of a macrophage cell. The movement was stopped in close prox-

imity to the membrane, and the position fluctuations during and after the binding of the bead to the cell membrane were measured.

In order to minimize signal contributions from, e.g., intracellular organelles or even the cell nucleus, we approached the cell periphery mainly from lateral directions as shown in the sketch of Fig. 1.

We investigated whether the cell membrane has any perturbing effects on the position detection signals. We verified that the position detection system works properly not only in bulk solution, but also during and after binding to the membrane in the following way: For all measurements, we calibrated the position detection system while the bead was trapped in bulk solution by using the Langevin method [7,32]. In a series of experiments we calibrated the system additionally by an independent method: Once the bead was bound to the membrane, we displaced the bead abruptly (within 50 ms) by 100 nm several times in all three directions by moving the piezodriven sample stage. The defined 100-nm jumps in the three position signals were used to calibrate the signals. Both calibration methods led to the same result, showing that the light scattered by the membrane is negligible compared to the light scattered by the 1-μm latex bead.

C. Results

1. Binding time point

A typical phagocytic binding event is shown in Fig. 7. Here, a LPS-coated bead was approached to a RAW macrophage cell in order to bind to the cell's plasma membrane. Displayed are the bead's x (a) and z (b) positions as a function of time taken at a sampling rate of 50 kHz. It can be seen that the bead's position remains within the unique detection range for $NA_{trap}=1.06$ [laterally ±320 nm (a), 770 nm in the $+z$, and 1400 nm in the $-z$ direction (b)].

In order to determine the time point when the bead binds to the cell membrane, the position fluctuations as a function of time were analyzed. The standard deviation σ_z (data not shown) of the bead's z position was determined in steps of 125 ms for overlapping time windows of 500 ms (25000 data points). For $t<9.25$ s, the bead was fluctuating in the trap in bulk solution with constant σ_z with an average value $\langle\sigma_z\rangle=85\pm7$ nm. For $t>9.75$ s, the fluctuations were strongly decreased to $\langle\sigma_z\rangle=27\pm6$ nm. In the transition region $t_0=9.5\pm0.25$ s, the fluctuations were continuously decreased from $\sigma_z=85$ to 27 nm. We associate this transition region with the time point of binding to the membrane defined by σ_z. This transition region is underlaid with dark gray in (b)–(d).

Instead of looking at the σ values, another means to determine the time point of binding is the autocorrelation time of the position signals. For a spherical particle diffusing in a harmonic potential, the autocorrelation function of its position decays exponentially [43]. In the case of a bead in a harmonic optical trap with a linear relation between the particle position i ($i=x,y,z$) and the position signal S_{ai}, the autocorrelation function of S_{ai} is also decaying exponentially,

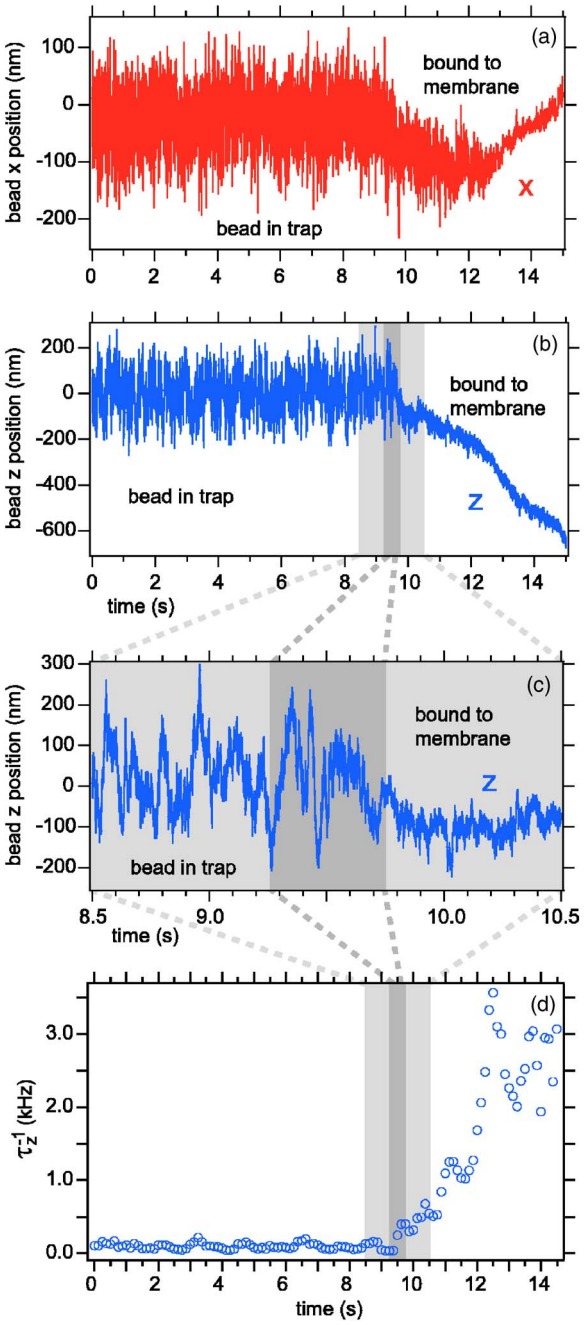

FIG. 7. (Color online) Position fluctuations of a LPS-bead binding to a RAW macrophage cell in the x (a) and z (b) directions. (a), (b) The bead is trapped in bulk solution for $t<9.5$ s. (b) At time point $t_1=9.5\pm0.1$ s the bead binds to the plasma membrane of the macrophage. About 1.0 s after binding, the bead is pulled downwards in the z direction with an average speed of 130 nm/s. (c) Cutout of the data from (b) for $t=(8.5,10.5)$ s. Shown is the transition from the unbound to the bound state. (d) The inverse autocorrelation time τ_z^{-1} of the z-position signal shows a strong increase at $t_1=9.5\pm0.1$ s.

$$\langle S_{ai}(t')S_{ai}(t'+t)\rangle \propto \exp(-t/\tau_i), \tag{5}$$

with an autocorrelation time $\tau_i=\gamma/\kappa_i$. Here $\gamma=6\pi r\eta$ is the viscous drag of the bead with radius r in a medium with a

viscosity η and $\kappa_i = \kappa_i^{tr}$ is the force constant of the trap. If the optically trapped bead is additionally attached to the cell membrane by a bond approximated by a linear spring with a force constant κ_i^b, the total force constant is $\kappa_i = \kappa_i^{tr} + \kappa_i^b$.

If an optically trapped particle is moved from bulk solution close to a cellular membrane, the particle starts to interact with the presumably viscoelastic extracellular matrix and potentially binds to the membrane. Therefore, assuming that the particle diffuses in a harmonic trap in a viscous medium is probably no longer a valid approximation. Nevertheless, $\langle S_{ai}(t')S_{ai}(t'+t)\rangle$ still shows an exponential decay in the millisecond range if the particle is in close vicinity to the cell membrane and if it is finally bound.

For that reason, τ_i can be used as a means to characterize the thermal motion of the bead also close to membranes. In Fig. 7(d) the inverse autocorrelation time τ_z^{-1} was determined in steps of 125 ms with overlapping time windows of 500 ms. During the first 9 s, where the bead is trapped in bulk solution, τ_z^{-1} is constant. At $t_1 = 9.5 \pm 0.1$ s the value τ_z^{-1} increases strongly. We associate this time interval with the time point of binding to the membrane defined by τ_z^{-1}.

The binding time points defined by σ_z and τ_z^{-1} yield the same value ($t_0 = 9.5 \pm 0.25$ s and $t_1 = 9.5 \pm 0.1$ s) but the precision is higher for the latter method. Moreover, nonlinearities in the position signals have a stronger disturbing effect on σ than on τ [16].

2. Transition from unbound to bound state

The high temporal sampling of the PFM is especially well suited to monitor the Brownian dynamics of the bead during the binding process. For example, the transition from the unbound state to the bound state in Fig. 7(c) occurs on a time scale on the order of about 100 ms. In order to measure an inverse autocorrelation time τ_0^{-1}, a sampling rate of about $10\tau_0^{-1}$ is necessary to achieve a good exponential fit. For a sampling rate of 50 kHz like in Fig. 7, inverse autocorrelation times up to 5 kHz can be measured.

In Fig. 8, the 3D position fluctuations of an IgG coated bead binding to a J774 macrophage cell are shown. The top graph displays the bead's position in the x, y, and z directions as a function of time. It can be seen that the bead's position remains within the unique detection range for $NA_{trap} = 1.06$. The transition from the unbound to the bound state occurs also on a time scale on the order of about 100 ms. The bottom graph shows 2D position histograms (xy and xz planes) for various time intervals. The first column for $t = (-3,1)$ s shows the position histograms of the bead fluctuating in the optical trap in bulk solution. The second column for $t = (1,3)$ s shows the transition from the bead fluctuating in the optical trap to a state where it is bound to the membrane. The binding occurs with an intermediate step (white arrowhead). This step is not only spatially separated as can be seen directly from the histogram, but also separates temporarily. It belongs to a small time window of $t = (2.3, 2.6)$ s. We assume that the bead is interacting with parts of the extracellular matrix during this intermediate step.

3. Initial mechanical response of the cell

Figure 7(b) shows that after binding to the membrane at $t = 9.5 \pm 0.1$ s, the bead is pulled downwards in the z direction with an average speed of 130 nm/s.

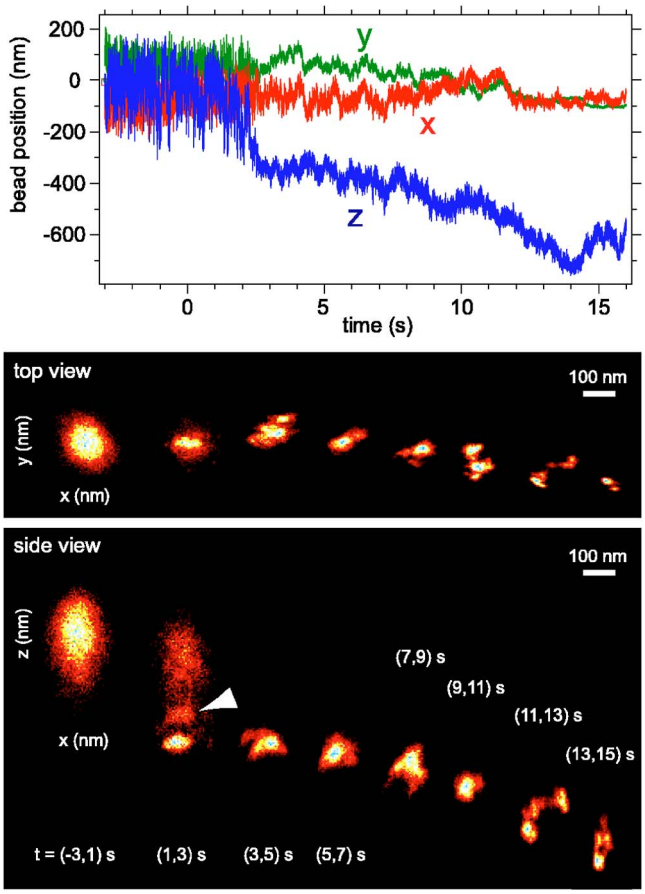

FIG. 8. (Color online) 3D bead positions for an IgG-bead binding to a J774 macrophage. Top graph: At time point $t = 2.3 \pm 0.1$ s the bead binds tightly to the membrane and is afterwards pulled downwards in the $-z$ direction. Lateral movements and oscillations on time and lengths scales of several tens of milliseconds and nanometers can be observed. Bottom graph: 2D position histograms (xy and xz planes) for various time intervals. The continuously recorded transition for $t = (1,3)$ s from the unbound to the bound state can be seen in the second column.

In Fig. 8 (top graph), upon binding at $t = 2.30 \pm 0.1$ s, the membrane pulls the bead downwards in the $-z$ direction with an average speed of 40 nm/s.

We investigated the initial mechanical response of the cell membrane during the first few seconds after binding for beads having different bound ligands. In total, we analyzed 118 binding experiments ($60\times$ IgG, $19\times$ complement, $19\times$ LPS, $20\times$ avidin). For all ligand-bead types, in most of the cases (53% IgG, 58% complement, 74% LPS, 55% avidin), the membrane pulled the bead *downwards* during the first few seconds after binding. Also for all bead types, a smaller fraction (22% IgG, 26% complement, 11% LPS, 25% avidin) showed an oscillatory up and down or an up and side movement of the bead and only a few cases (12% IgG, 11% complement, 0% LPS, 0% avidin) showed a pure *upwards* movement. In a couple of experiments, we measured the bead movement for about 3 min after the binding. In all cases, during this time interval the bead was moved by the membrane upwards, downwards and laterally on the order of 1 μm.

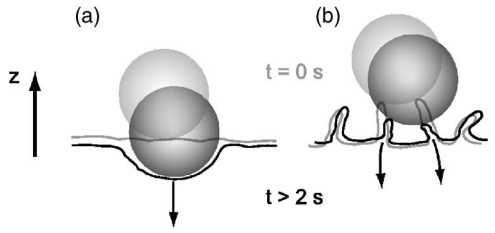

FIG. 9. (a) The most frequent membrane response upon binding was a downward pulling of the bead. The time delay between binding and response was on average 2 s. (b) Our observations led us to suggest that upon binding, small membrane protrusions (ruffles) retract and pull the bead downwards.

Noteworthy, independent of the bead type, the most frequent initial membrane response upon binding was a downwards pulling of the bead (Fig. 9).

4. Time delay between binding and mechanical membrane response

Figures 7(b) and 7(c) show that after binding to the membrane at $t=9.5\pm0.1$ s, the bead remains on average at the same z position for about 1.0 s until it is pulled downwards by the membrane. Analyzing 32 experiments, we found that the time delay Δt between binding and the following membrane response had a broad spectrum ranging from $\Delta t = 0.2$ s up to $\Delta t > 6$ s. The average value was $\langle \Delta t \rangle = 2$ s.

V. SUMMARY AND CONCLUSIONS

We measured the interferometric position signals of a 1-μm bead in the focus of a PFM for various trapping lens numerical apertures between $NA_{trap}=0.30$ and $NA_{trap}=1.20$. For the first time, these signals were compared to predictions based on an extended Mie theory [15,16]. Theory and experiment are in very good agreement. We showed that the relative radiation pressure and thereby the trapping position of the bead can be controlled by changing NA_{trap}. A variation of NA_{trap} causes a change of the mean incident axial photon momentum, which is equivalent to a variation of the mean axial wavelength of the laser in the focal region or a change of the Gouy-Phase shift. By varying the trapping position of the bead, the unique region of position detection and the degree of z dependence of the lateral signal sensitivities can be tuned for specific applications. For applications where only the lateral position detection of a (trapped) bead is important, a low NA_{trap} shows a bigger unique detector region and significantly less variations in the signal sensitivities. However, the smaller the NA_{trap}, the closer the trap position moves towards the nonlinear region for the axial signal. For experiments where stable 3D position detection is required, a compromise has to be found between small variations in the lateral signal sensitivities (low NA_{trap}) and longer unique axial detection range in the $+z$ (high NA_{trap}) and $-z$ directions (low NA_{trap}). We have chosen $NA_{trap}=1.06$ to optimize the 3D detection required for the membrane binding experiments described in this article. Compared to $NA_{trap}=1.20$ this yields a decrease in the lateral signal sensitivity variations of 50%.

We used the improved 3D tracking capacity of the PFM to investigate the binding of optically trapped beads to the plasma membrane of macrophage cells. One could use a simple optical tweezer setup in combination with video microscopy particle tracking to perform similar experiments. However, video microscopy has typical sampling rates below 100 Hz and requires cumbersome defocusing methods for particle tracking in axial direction. Using defocusing techniques for particle tracking, not only the particle itself but also the sample is defocused. In contrast, the PFM decouples particle tracking from video imaging of the sample. This allows an independent observation of the sample using common microscopy techniques in parallel to high-precision particle tracking.

We studied the binding of variously coated beads to the plasma membrane of living macrophage cells preceding phagocytosis. We used J774 and RAW mouse macrophages and beads coated with IgG, complement, LPS, or avidin, which except for avidin interact with known cell surface receptors. Using a low trapping laser power of about 2 mW in the focal region, the event of binding to the membrane is characterized by a strong decrease in the position fluctuations σ_i of the bead. In addition, the binding is characterized by a strong increase of the inverse position signal autocorrelation time τ_i^{-1}. The 3D spatial behavior (σ_i), as well as the temporal behavior (τ_i^{-1}) can be easily measured simultaneously by photonic force microscopy with its tracking precision of a few nanometers and a used sampling rate of 10–50 kHz. After binding, the membrane shows an active response and moves the bound bead away from the trap position. Independent of the bead coating (IgG, complement, LPS, avidin), in most cases (58%) the membrane pulled the bead downwards in the $-z$ direction during the first few seconds after binding [Fig. 9(a)]. In a smaller number of cases (21%) the bead showed an oscillatory up and down or an up and side movement and only rarely (8%) a pure upwards movement was observed. The time delay Δt between binding and the mechanical membrane response had a broad range from very fast $\Delta t=0.2$ s up to $\Delta t > 6$ s with an average value of $\langle \Delta t \rangle = 2$ s [Fig. 9(a)].

We observed that membrane protrusions extending from the membrane in the lateral direction always retracted and pulled the bead towards the membrane upon binding. These protrusions were not only at those sites where the cell is attached to the coverslip, but also freely moving several micrometers above the coverslip. Small protrusions or ruffles that are several hundred nanometers in length and extend perpendicular to the membrane mainly in axial direction are not visible by DIC microscopy. However, due to the observation that most of the cells we observed possess protrusions visible in the periphery of the cell if they extend in the lateral direction, we assume that there are also small protrusions or "ruffles" extending in the axial direction. Starting from our result that the most frequent initial membrane response during the first few seconds is a downward pulling of the bead, we suggest that small protrusions or ruffles are involved in this process [Fig. 9(b)].

Given that the molecular signaling response from different phagocyte receptors is known to be unique for each re-

ceptor [23,24,39,44] one might expect significant differences in the initial membrane response upon binding. In particular, it is widely believed [36,37] that the membrane morphology during the wrapping process, which takes several minutes, is different for IgG and complement particles. However, in our study, we did not find a significant difference in the initial membrane response during the first few seconds for the various ligand beads (IgG, complement, LPS, avidin). Our result suggest that the earliest events in phagocytosis share are a common mechanism.

ACKNOWLEDGMENTS

This work was partially supported by the German National Academic Foundation (Studienstiftung des deutschen Volkes). The authors thank Siegfried Winkler at EMBL's electronic workshop for the development of the sample heating system, Dirk Neumayer for software development, and Daniela Holzer and Mark P. Kühnel for providing the beads and helpful comments.

[1] A. Ashkin, J. M. Dziedzic, J. E. Bjorkholm, and S. Chu, Opt. Lett. **11**, 288 (1986).
[2] M. J. Lang and S. M. Block, Am. J. Phys. **71**, 201 (2003).
[3] K. C. Neuman and S. M. Block, Rev. Sci. Instrum. **75**, 2787 (2004).
[4] I. M. Peters, B. G. de Grooth, J. M. Schins, C. G. Figdor, and J. Greve, Rev. Sci. Instrum. **69**, 2762 (1998).
[5] M. E. J. Friese, A. G. Truscott, H. Rubinsztein-Dunlop, and N. R. Heckenberg, Appl. Opt. **38**, 6597 (1999).
[6] A. Pralle, M. Prummer, E.-L. Florin, E. H. K. Stelzer, and J. K. H. Hörber, Microsc. Res. Tech. **44**, 378 (1999).
[7] A. Rohrbach, C. Tischer, D. Neumayer, E.-L. Florin, and E. H. K. Stelzer, Rev. Sci. Instrum. **75**, 2197 (2004).
[8] E.-L. Florin, J. K. H. Hörber, and E. H. K. Stelzer, US patent No. US 6,833,923 B3, 2005.
[9] A. Pralle, P. Keller, E.-L. Florin, K. Simons, and J. K. H. Hörber, J. Cell Biol. **148**, 997 (2000).
[10] C. Tischer, S. M. Altmann, S. Fišinger, J. K. H. Hörber, E. H. K. Stelzer, and E.-L. Florin, Appl. Phys. Lett. **79**, 3878 (2001).
[11] S. Jeney, E. H. K. Stelzer, H. Grubmüller, and E.-L. Florin, ChemPhysChem **5**, 1150 (2004).
[12] N. B. Becker, S. M. Altmann, T. Scholz, J. K. H. Hörber, E. H. K. Stelzer, and A. Rohrbach, Phys. Rev. E **71**, 021907 (2005).
[13] M. W. Allersma, F. Gittes, M. J. deCastro, R. J. Stewart, and C. F. Schmidt, Biophys. J. **74**, 1074 (1998).
[14] I. M. Tolić-Nørrelykke, E.-L. Munteanu, G. Thon, L. Oddershede, and K. Berg-Sørensen, Phys. Rev. Lett. **93**, 078102 (2004).
[15] A. Rohrbach and E. H. K. Stelzer, J. Appl. Phys. **91**, 5474 (2002).
[16] A. Rohrbach, H. Kress, and E. H. K. Stelzer, Opt. Lett. **28**, 411 (2003).
[17] C. Tischer, A. Pralle, and E.-L. Florin, Microsc. Microanal. **10**, 1 (2004).
[18] K. Visscher and S. M. Block, Methods Enzymol. **298**, 460 (1998).
[19] K. Visscher, M. J. Schnitzer, and S. M. Block, Nature (London) **400**, 184 (1999).
[20] J. K. Dreyer, K. Berg-Sørensen, and L. Oddershede, Appl. Opt. **43**, 1991 (2004).
[21] L. G. Gouy, Acad. Sci., Paris, C. R. **110**, 1251 (1890).
[22] M. Born and E. Wolf, *Principles of Optics* (Cambridge University Press, New York, 1999).
[23] A. Aderem and D. M. Underhill, Annu. Rev. Immunol. **17**, 593 (1999).
[24] S. Greenberg and S. C. Silverstein, in *Fundamental Imnmnology*, 3rd ed., edited by W. E. Paul (Raven Press Ltd., New York, 1993), p. 941.
[25] M. Desjardins and G. Griffiths, Curr. Opin. Cell Biol. **15**, 498 (2003).
[26] A. Caspi, O. Yeger, I. Grosheva, A. D. Bershadsky, and M. Elbaum, Biophys. J. **81**, 1990 (2001).
[27] A. Caspi, R. Granek, and M. Elbaum, Phys. Rev. E **66**, 011916 (2002).
[28] D. Choquet, D. P. Felsenfeld, and M. P. Sheetz, Cell **88**, 39 (1997).
[29] F. Takahashi, Y. Higashino, and H. Miyata, Biophys. J. **84**, 2664 (2003).
[30] H. Kress, E. H. K. Stelzer, and A. Rohrbach, Appl. Phys. Lett. **84**, 4271 (2004).
[31] M. J. Lang, C. L. Asbury, J. W. Shaevitz, and S. M. Block, Biophys. J. **83**, 491 (2002).
[32] E.-L. Florin, A. Pralle, E. H. K. Stelzer, and J. K. H. Hörber, Appl. Phys. A: Mater. Sci. Process. **66**, S75 (1998).
[33] A. Rohrbach and E. H. K. Stelzer, J. Opt. Soc. Am. A **18**, 839 (2001).
[34] A. Rohrbach, H. Kress, and E. H. K. Stelzer, Appl. Opt. **43**, 1827 (2004).
[35] S. C. Kuo and J. L. McGrath, Nature (London) **407**, 1026 (2000).
[36] J. A. Swanson and C. S. Baer, Trends Cell Biol. **5**, 89 (1995).
[37] A. H. Allen and A. Aderem, J. Exp. Med. **184**, 627 (1996).
[38] G. Kaplan, Scand. J. Immunol. **6**, 797 (1977).
[39] J. A. Swanson and A. D. Hoppe, J. Leukoc Biol. **76**, 1093 (2004).
[40] M. Desjardins, L. A. Huber, R. G. Parton, and G. Griffiths, J. Cell Biol. **124**, 677 (1994).
[41] R. M. Henry, A. D. Hoppe, N. Joshi, and J. A. Swanson, J. Cell Biol. **164**, 185 (2004).
[42] A. A. Aderem, S. D. Wrigth, S. C. Silverstein, and Z. A. Cohn, J. Exp. Med. **161**, 617 (1985).
[43] F. Reif, *Fundamentals of Stastistical and Thermal Physics* (McGraw-Hill, Singapore, 1985).
[44] S. Greenberg and S. Grinstein, Curr. Opin. Immunol. **14**, 136 (2002).